Computational and Structural Biotechnology Journal 17 (2019) 527–536

COMPUTATIONAL AND STRUCTURAL BIOTECHNOLOGY JOURNAL

journal homepage: www.elsevier.com/locate/csbj

DNA *i*-Motifs With Guanidino-*i*-Clamp Residues: The Counterplay Between Kinetics and Thermodynamics and Implications for the Design of pH Sensors

Vladimir B. Tsvetkov [a,b,c], Timofei S. Zatsepin [d,e], Anton V. Turaev [a,f], Valentina M. Farzan [d], Galina E. Pozmogova [a,g], Andrey V. Aralov [h,*], Anna M. Varizhuk [a,i,**]

[a] Research and Clinical Center for Physical Chemical Medicine, Malaya Pirogovskaya str. 1a, Moscow 119435, Russia
[b] I.M. Sechenov First Moscow State Medical University, Trubetskaya Str. 8-2, 119991 Moscow, Russia
[c] Research Institute of Influenza, Professora Popova str., 15/17, Sankt-Peterburg 197376, Russia
[d] Skolkovo Institute of Science and Technology, Skolkovo, 143026 Moscow, Russia
[e] Lomonosov Moscow State University, Department of Chemistry, Leninskie Gory Str. 1-3, 119992 Moscow, Russia
[f] Moscow Institute of Physics and Technology, Institutsky lane 9, Dolgoprudny 141700, Russia
[g] Institute of Bioengineering, Research Center of Biotechnology of the Russian Academy of Sciences, Leninsky prospect, 33, build. 2, Moscow 119071, Russia
[h] Shemyakin-Ovchinnikov Institute of Bioorganic Chemistry, Russian Academy of Sciences, Miklukho-Maklaya str. 16/10, Moscow 117997, Russia
[i] Engelhardt Institute of Molecular Biology, Russian Academy of Sciences, Vavilov str. 32, Moscow 119991, Russia

ARTICLE INFO

Article history:
Received 27 February 2019
Received in revised form 8 April 2019
Accepted 10 April 2019
Available online 13 April 2019

Keywords:
DNA secondary structure
I-motif
Phenoxazine derivative
Thermal stability
Kinetics
pH sensor

ABSTRACT

I-motif structures, adopted by cytosine-rich DNA strands, have attracted considerable interest as possible regulatory elements in genomes. Applied science exploits the advantages of *i*-motif stabilization under acidic conditions: *i*-motif-based pH sensors and other biocompatible nanodevices are being developed. Two key characteristics of *i*-motifs as core elements of nanodevices, *i.e.*, their stability under physiological conditions and folding/unfolding rates, still need to be improved. We have previously reported a phenoxazine derivative (*i*-clamp) that enhances the thermal stability of the *i*-motif and shifts the pH transition point closer to physiological values. Here, we performed *i*-clamp guanidinylation to further explore the prospects of clamp-like modifications in *i*-motif fine-tuning. Based on molecular modeling data, we concluded that clamp guanidinylation facilitated interstrand interactions in an *i*-motif core and ultimately stabilized the *i*-motif structure. We tested the effects of guanidino-*i*-clamp insertions on the thermal stabilities of genomic and model *i*-motifs. We also investigated the folding/unfolding kinetics of native and modified *i*-motifs under moderate, physiologically relevant pH alterations. We demonstrated fast folding/unfolding of native genomic and model *i*-motifs in response to pH stimuli. This finding supports the concept of *i*-motifs as possible genomic regulatory elements and encourages the future design of rapid-response pH probes based on such structures. Incorporation of guanidino-*i*-clamp residues at/near the 5′-terminus of *i*-motifs dramatically decreased the apparent unfolding rates and increased the thermal stabilities of the structures. This counterplay between the effects of modifications on *i*-motif stability and their effects on kinetics should be taken into account in the design of pH sensors.

© 2019 The Authors. Published by Elsevier B.V. on behalf of Research Network of Computational and Structural Biotechnology. This is an open access article under the CC BY-NC-ND license (http://creativecommons.org/licenses/by-nc-nd/4.0/).

1. Introduction

Recent findings advocate the *in vivo* existence of i-motifs (IMs) – intercalated parallel duplexes that are stabilized by hemi-protonated cytosine pairs [1] – in genomic DNA [2] and confirm that preassembled exogenous IMs can sustain intracellular conditions [3]. These findings have stimulated fundamental studies of the roles of genomic IMs and highlighted the prospects of synthetic IMs as biocompatible pH-sensitive tools for *in vivo* studies. The major results of fundamental studies of IMs were comprehensively reviewed in 2018 [4]. Typically, IMs are stable at mildly acidic pH [5,6]. Each IM has a characteristic pH transition value (pHi - pH, at which half of the structure is folded). The structural features that determine IM pH sensitivity and thermal stability include *(i)* the number of C-C^+ pairs (the size of the IM core) [7–9], which affects the cooperativity of cytosine protonation/deprotonation;

* Correspondence to: A.V. Aralov, Miklukho-Maklaya str. 16/10, Moscow 117997, Russia.
** Correspondence to: A.M. Varizhuk, Malaya Pirogovaskaya str. 1A, Moscow 119435, Russia.
E-mail addresses: Baruh238@gmail.com (A.V. Aralov), annavarizhuk@gmail.com (A.M. Varizhuk).

https://doi.org/10.1016/j.csbj.2019.04.006
2001-0370/© 2019 The Authors. Published by Elsevier B.V. on behalf of Research Network of Computational and Structural Biotechnology. This is an open access article under the CC BY-NC-ND license (http://creativecommons.org/licenses/by-nc-nd/4.0/).

(ii) the groove geometry [10] (destabilizing phosphate-phosphate interactions are compensated by stabilizing sugar contacts); and *(iii)* core-flanking nucleotides in loops [11] and additional non-canonical structural elements. The primary external factors that affect IM stability are pH, solution ionic strength and molecular crowding [12]. The key factor that presumably facilitates IM folding in the context of genomic DNA is torsion stress [13].

Advances in practical applications of IMs (mainly as elements of pH probes, hydrogels or nanomachines) have been summarized in several elegant reviews [14–18]. Notable recent examples of IM-based molecular tools and nanomachines include programmable *i*-switches, proton-sensitive ionic channels combined with chemical oscillators, containers for drug delivery and pH-controlled drug release, among others [19–23]. In the context of biosensor technologies, the design of IM-based pH probes for *in vivo* applications is a particularly popular trend. The first successful application of an IM-based pH probe (an intermolecular DNA construct labeled with FRET pairs) in living cells was reported in 2009 [24], and later, the functionality of the probe was demonstrated in *C. elegans* [25]. The probe had a relatively narrow dynamic range (pH 5.8–6.8) and was used to monitor endosome maturation. In a follow-up study, the design of the probe was optimized to enable simultaneous visualization of two partially orthogonal and partially overlapping endocytosis pathways [26]. Since then, there has been a ceaseless interest in IMs with respect to intracellular pH sensing. An example of a recently developed probe is a DNA construct prone to IM-duplex transitions that contains fluorescent labels and a quencher. Distinct fluorophores are quenched in the IM and duplex states, which produces a ratiometric pH probe with a rather high dynamic range [27]. It should be noted that although all of the above examples are based on fluorescent detection, other variants are also being considered and include IM-harboring sensors for Raman spectroscopy and colorimetric detection [28–30]. To summarize, there has been apparent progress in the development of IM-harboring nanodevices. However, two important features of IM-based pH-sensitive elements – the pH-tolerance range (basically, the pH transition point) and response rates (basically, folding/unfolding kinetics) – still require fine tuning for wide application.

Available IM-based probes exhibit relatively slow kinetics with typical response times of several seconds to minutes [24–26], which are probably consequences of the relatively complex IM designs and utilization of intermolecular IM structures. It has been argued that intramolecular IM-based sensors may be able to provide more rapid responses to pH alterations [31]. Thus, further improvements require detailed studies of the IM folding/unfolding kinetics, ideally under moderate pH alterations within the physiologically relevant range. A recent analysis of the human genome has revealed that there are multiple sequences capable of IM formation under near-physiological conditions [32], and ongoing studies may provide more examples [33,34]. Stable genomic structures appear to be good candidates for the development of biocompatible intramolecular IM-based pH-sensitive tools. Chemical modification can be used for their additional optimization, *i.e.*, to fine-tune pHi and enhance thermal stability in neutral solutions. We have previously reported a modification (incorporation of *i*-clamp residues close to the 5′-terminus of IMs) that increased the pHi value of model IMs, enhanced the thermal stability of model IMs in mildly acidic solutions and enhanced the thermal stability of a genomic IM in a neutral solution [35]. This modification seems to be promising (along with several other modifications reviewed recently [4]) in regard to fine-tuning IM-based sensors.

Here, we continued to study clamp-based modifications. We explored the prospects of *i*-motif optimization *via i*-clamp guanidinylation. We started by verifying our assumption about the benefits of *i*-clamp guanidinylation *in silico* (molecular modeling). Next, we analyzed the effects of guanidino-*i*-clamp insertions in IMs by optical methods (absorption and circular dichroism spectroscopy) and directly compared the results with those obtained previously for *i*-clamp. Finally, we investigated the folding/unfolding kinetics of native and modified IMs under moderate, near-physiological pH jumps (stopped-flow experiments) to evaluate the applicability of these structures for the development of rapid-response pH probes.

2. Materials and Methods

2.1. Molecular Modeling

Molecular models of tetramolecular IMs with *i*-clamp (T1Z) or guanidino-*i*-clamp (T1Zg) insertions (see Fig. 1A for schemes and Table 1 for sequences of the modified IMs and their native analog To) were constructed as described in the literature [35]. Briefly, we first combined structural elements of two well-characterized tetramolecular IMs (PDB_1YBL and PDB_2N89) using Sybyl-X software (Certara, USA) and optimized the resulting structure to obtain the native IM To. Next, we replaced C2 cytosine residues in To by the i-clamp residues and reoptimized the structure to obtain T1Z. Finally, we replaced the amino group of the aminopropyl tether in i-clamp by the guanidino group and performed the last round of conformational optimization to obtain T1Zg. Optimization at each step was performed using Sybyl-X software and Powell's method (for more details, see [9]). Calculations of the partial charges for modified nucleotides, model optimization, molecular dynamics (MD) simulations and free energy calculations were performed as previously described [35].

2.2. Oligonucleotide Synthesis, Purification and Mass-Spectrometry Analysis

To prepare and characterize guanidinylated *i*-clamp oligonucleotides (ODNs), synthesis of *i*-clamp ODNs followed by postsynthetic guanidinylation, purification and MS analysis was performed according to previously published procedures [35,36]. The guanidinylated *i*-clamp ODNs included T1Zg, U1Zg, M1Zg, M6Zg, G1Zg and G2Zg. See Table 1 for their sequences and the supplementary information for their MS and HPLC data (Table S1, ESI-MS spectra and HPLC traces). The *i*-clamp ODNs T1Z (analog of the native tetramolecular IM To), U1Zg (analog of the native unimolecular IM Uo), M1Zg and M6Zg (analogs of the native model IM Mo), and G1Zg and G2Zg (analogs of the native genomic IM Go) have been characterized previously [35]. Native IMs To, Uo, Mo and Go were purchased from Litekh, Russia (purity≥95% by HPLC).

2.3. Absorption and Circular Dichroism Spectroscopy

ODNs were dissolved in 10 mM sodium phosphate buffer (pH 5.8 for To, Uo and their derivatives and pH 7.4 for Go, Mo and their derivatives). The Uo and U1Z samples were rapidly annealed (heated to 95 °C for 5 min and then cooled on ice to facilitate intramolecular folding) prior to the experiments, and the other samples were slowly annealed (heated to 95 °C and then cooled gradually to room temperature). The ODN concentrations were 10 μM (To and T1Z) or 5 μM (other ODNs). The absorption spectra, circular dichroism (CD) spectra and melting/annealing curves of the ODNs were recorded on a Chirascan spectrophotometer (Applied Photophysics, UK) equipped with a thermostated cuvette-holder as previously described [35], and thermal difference spectra (TDS) were obtained by subtracting the absorption spectra at 5 °C from the spectra at 90 °C. Melting and annealing temperatures were determined from the maxima of the first derivatives of the melting curves. The heating/cooling rates were 1 °C/min.

2.4. Stopped-Flow Experiments

Stopped-flow measurements with monitoring by CD (CDSF) were carried out at 25 °C on a Chirascan spectrophotometer (Applied Photophysics) equipped with a stopped-flow accessory with a 10 mm optical path. CD was recorded at 288 nm, and the bandwidth was set

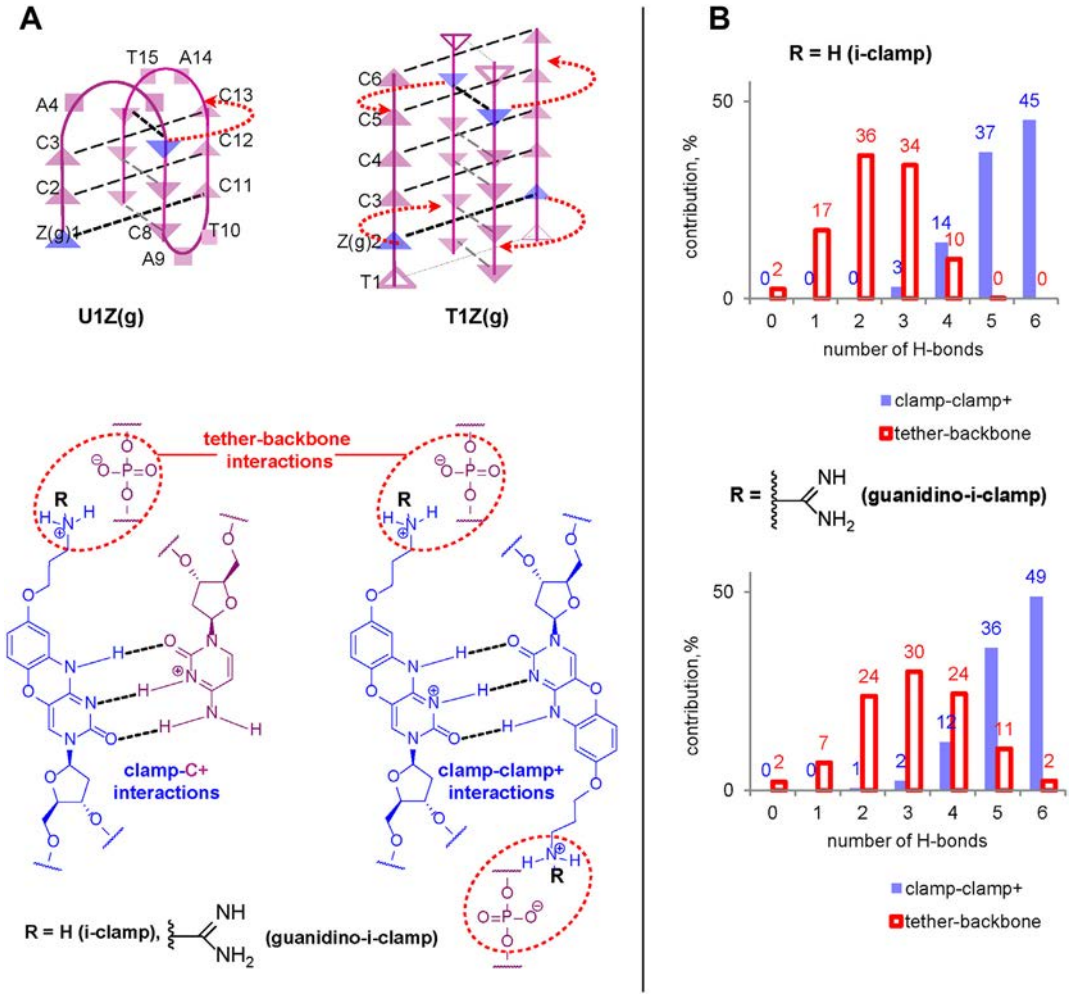

Fig. 1. i-Clamp *versus* guanidino-*i*-clamp: general schemes of the IMs and a H-bonding summary (from MD simulations). A – Schematic representations of the presumed intramolecular (U1Z and U1Zg) and tetramolecular (T1Z and T1Zg) IM structures (top panel) with clamp–cytosine$^+$ (U1Z and U1Zg) and clamp–clamp$^+$ (T1Z and T1Zg) pairs (bottom panel). B – Summary of the H-bonding efficiency in T1Z (top panel) and T1Zg (bottom panel) based on the MD simulation results. The contributions of snapshots with different overall numbers of H-bonds in the clamp–clamp+ pairs (red histograms) or between the clamp tethers and the backbones of the neighboring strands (blue histograms) are given as percentages from the total number of snapshots from the MD simulation trajectory.

to 6 nm. In all CDSF experiments, the preannealed ODN samples (rapid preannealing for Uo and U1Z and slow preannealing for other ODNs) in 50 mM sodium phosphate buffer were rapidly mixed (1: 4) with 80 mM sodium phosphate buffer of a different pH (4.5 or 9.0). There were four series of CDSF measurements:

1) 6.8 → 5.7 pH jump (for To, T1Zg, Uo and U1Zg). The ODN solution (70 μM for To and T1Zg, 15 μM for Uo and U1Zg) in 50 mM sodium phosphate, pH 6.8, was mixed (1:4) with 80 mM sodium phosphate, pH 4.5, to a final sodium phosphate concentration of 74 mM, pH 5.7.

Table 1
IM sequences, melting temperatures and annealing temperatures.

Code	Sequence	Tm[a] (±1 °C)	ΔTm[b] (±2 °C)	Ta (±1 °C)	ΔTa[b] (±2 °C)
To	TCCCCC	47	–	ND[c]	–
T1Zg	T**Zg**CCCC	53	+6	ND[c]	–
Uo	CCCATCCCATCCCATCCC	39	–	37	–
U1Zg	**Zg**CCAT**Zg**CCATCCCATCCC	46	+7	ND[d]	–
Mo	CCCCCTTCCCCCTTCCCCCTTCCCCC	20	–	≤8	–
M1Zg	**Zg**CCCCTTCCCCCTTCCCCCTTCCCCC	22	+2	11	+3
M6Zg	CCCCCTTCCCCCTTCCCCCTTCCCC**Zg**	19	−1	9	+1
Go	CCCCCCTCCCCCCCTCCCCCCTCCCCCC	26	–	10	–
G1Zg	**Zg**CCCCCTCCCCCCCTCCCCCCTCCCCCC	28	+2	13	+3
G2Zg	CCCCCCTCCC**Zg**CCCTCCCCCCTCCCCCC	21	−5	10	0

[a] Conditions: 10 mM sodium phosphate (pH 7.4) and 100 mM NaCl (Go, Mo and their analogues) or 10 mM sodium phosphate, pH 5.8 (To, Uo and their analogues). ON concentrations: 10 μM (To and T1Zg) or 5 μM (the rest).
[b] Modification-induced changes of IM thermal stability: $\Delta Tm/a = Tm/a^{\text{modified IM}} - Tm/a^{\text{native IM}}$.
[c] The annealing temperature could not be determined because hysteresis was too large.
[d] The annealing temperature could not be determined accurately because of the ambiguous annealing curve, which is presumably due to non-cooperative folding and/or conformational polymorphism.

2) 5.2 → 7.5 pH jump (for To, T1Zg, Uo and U1Zg). The ODN solution (70 μM for To and T1Zg, 15 μM for Uo and U1Zg) in 50 mM sodium phosphate, pH 5.2, was mixed (1:4) with 80 mM sodium phosphate, pH 9.0, to a final sodium phosphate concentration of 74 mM, pH 7.5.
3) 8.0 → 6.0 pH jump (for Go, G1Zg, G2Zg, Mo, M1Zg and M6Zg). The ODN solution (15 μM) in 50 mM sodium phosphate, pH 8.0, containing 90 mM NaCl, was mixed (1:4) with 80 mM sodium phosphate, pH 4.5, that also contained 90 mM NaCl to a final sodium phosphate concentration of 74 mM, pH 6.0.
4) 6.7 → 7.9 pH jump (for Go, G1Zg, G2Zg, Mo, M1Zg and M6Zg). The ODN solution (15 μM) in 50 mM sodium phosphate, pH 6.7, containing 90 mM NaCl, was mixed (1:4) with 80 mM sodium phosphate, pH 9.0, that also contained 90 mM NaCl to a final sodium phosphate concentration of 74 mM, pH 7.9.

Each experiment was performed at least in triplicate; the resulting kinetic curves were averaged and fitted to single exponentials using ProData software (Applied Photophysics, UK).

3. Results and Discussion

3.1. Molecular Dynamics of Clamp-Harboring i-Motifs: i-Clamp Versus Guanidino-i-Clamp In Silico

i-Clamp, a phenoxazine derivative with a C8-aminopropyl (8AP) tether, has previously been incorporated [35] into ODNs to form unimolecular (Uo) or tetramolecular (To) IMs that are stable under mildly acidic conditions (pHi = 6.0 ± 0.1 and 5.8 ± 0.1 for Uo and To, respectively, in a low ionic strength buffer [35]) and into model (Mo) and genomic (Go) IMs that sustain near-physiological conditions (pHi = 7.1 for Mo and Go in a near-physiological ionic strength buffer [32]). The sequences of the ODNs are given in Table 1. The *i*-clamp modification enhanced the thermal stabilities of the IMs when introduced at the 5′ terminus of the ODNs, and the increase in the IM melting temperature (ΔTm) was up to +5 °C. This stabilizing effect was attributed (at least in part) to the electrostatic interactions between the 8AMP tether and the neighboring strand backbone (phosphate residues). Importantly, those interactions did not compromise the formation of *i*-clamp–C^+ pairs (*e.g.*, in a Uo derivative, U1Z) or *i*-clamp–*i*-clamp+ pairs (*e.g.*, in a To derivative, T1Z). Schematic representations of the IMs and the presumed clamp–C^+ and clamp–clamp$^+$ pairs are shown in Fig. 1A. Previously reported MD simulation results supported the schemes shown in Fig. 1A but indicated that the efficiency of the tether-backbone interactions was moderate. For instance, in the case of T1Z, only one of two possible tether-backbone bonds per clamp–clamp$^+$ pair was observed in most snapshots [35]. We analyzed a rather short MD trajectory in the initial study [35]; therefore, for a more detailed analysis, we doubled the simulation time. The major results of the detailed analysis of the tether-backbone interaction efficiency in T1Z (relative contributions of the snapshots with different total, rather than the normalized per clamp–clamp$^+$ pair, numbers of H-bonds) are shown in Fig. 1B, top graph. The 12 ns T1Z snapshot is shown in Fig. 2A, left panel. The root mean square deviation (RMSD) time plot, which indicates stability of the T1Z structure throughout the simulation, is shown in Fig. 2B; and the H-bonding time plots are shown in Fig. 2C.

The results of the detailed analysis were generally in line with previously observed tendencies [35]; therefore, we concluded that further increasing the simulation time was unnecessary. As summarized in Fig. 1B, top graph, both clamp–clamp$^+$ pairs were frequently (45% of snapshots) held together by 3H-bonds each (6 clamp–clamp$^+$ bonds in total for T1Z) and thus appeared to be stable. Regarding the tether-backbone interactions, snapshots with 1H-bond per pair (2 tether-backbone bonds in total for T1Z) were the most frequent (36%). This result is clearly suboptimal. We assumed that the tether-backbone interactions could be enhanced by replacing the aminopropyl group (8AP) with a guanidinopropyl group (8GP) and performed MD simulations for the respective T1Z analog (T1Zg). The phenoxazine derivative with the 8GP tether is hereafter referred to as the guanidino-*i*-clamp (see Fig. 1A for the structure of the guanidino-*i*-clamp and scheme of T1Zg and Table 1 for the sequence of T1Zg). The major results of the T1Zg MD simulation are given in Fig. 1B, bottom panel (H-bonding summary). The 12 ns snapshot, RMSD time plot, and the H-bonding time plots are shown in Fig. 2A-C, right panel. The data in Figs. 1A and 2C suggest that the tether-backbone interactions were strengthened in T1Zg. The snapshots with 3 tether-backbone H-bonds were the most frequent (30%), and the contribution of the snapshots with 4 tether-backbone H-bonds increased compared to that with T1Z (24% *vs.* 10%). Interestingly, the clamp–clamp$^+$ pairing efficiency was also improved: the contribution of snapshots with 6 clamp-clamp$^+$ bonds in total increased to 49% (Fig. 1B).

To summarize this section, guanidino-*i*-clamp seems to be superior to *i*-clamp in terms of H-bonding. Similar conclusions were drawn based on the analysis of electrostatic contributions to free energies. The 8GP-tether has a generally enhanced potential for coulomb interactions. The time plots of the average tether-backbone electrostatic energies (Fig. 3A, right graph) clearly illustrate the benefits of replacing the 8AP tether with 8GP (after substantial fluctuations during the first 10 ns of the simulations, the Eeq difference settled down to approximately 20 kcal/mol). Minor benefits in terms of the average tether-backbone van der Waals energy (Fig. 3A, left graph) were also observed (the difference was approximately 1 kcal/mol). The strengthened tether-backbone interactions dragged the phenoxazine residues to be slightly closer to each other in clamp–clamp$^+$ (Fig. 3B), thus enabling more efficient interactions between them in T1Zg compared with T1Z. While the van der Waals contributions to clamp–clamp$^+$ pairing were negligible (Fig. 3C, left graph) and roughly similar in T1Z and T1Zg, the difference in the electrostatic contributions was minor, but noticeable – approximately 0.5 kcal/mol (Fig. 3C, right graph).

We would like to emphasize that the benefits of replacing the 8AP clamp tether with 8GP were moderate in our molecular modeling experiments. The overall H-bonding efficiency difference between *i*-clamp and guanidino-*i*-clamp was less pronounced than that between *i*-clamp and G-clamp [35]. We could not directly correlate these differences with the IM-stabilizing effects (ΔTm). However, we could arguably conclude that guanidino-*i*-clamp is a promising modification according to the *in silico* tests. We expected its stabilizing effects in IMs to be superior or close to those of *i*-clamp, so we next tested guanidino-*i*-clamp *in vitro*.

3.2. Effects of Guanidino-i-Clamp Insertions on the Thermal Stabilities of Model and Genomic i-Motifs: i-Clamp Versus Guanidino i-Clamp In Vitro

We synthesized the guanidino-*i*-clamp derivatives of the previously reported *i*-clamp-bearing IMs [35] (Table 1) and analyzed their thermal stabilities under previously used conditions: pH 5.8 for Uo and To derivatives (presumably unimolecular and tetramolecular structures, respectively, which are folded under mildly acidic solutions) and pH 7.4 for the derivatives of model (Mo) and genomic (Go) IMs, which sustain near-physiological conditions [32].

The CD spectra, TDS and melting/annealing curves of the guanidino-*i*-clamp-IMs are shown in Fig. 4. Both CD spectra (Fig. 4A) and TDS (Fig. 4B) contained the characteristic features of IM structures: positive CD bands near 285–288 nm [5] and negative TDS bands near 295 nm [37]. The spectrum of the modified ODN U1Zg differed substantially from that of the native analog Uo: the positive band was broadened and a minor arm near 275 nm (attributable to the unfolded ODN fraction) was apparent along with the major peak near 285 nm. The increased hysteresis (Fig. 4C) suggests that the folded U1Zg structure may be different from that of Uo (*e.g.*, an intermolecular IM may be formed). Moreover, the shape of the annealing curve was somewhat

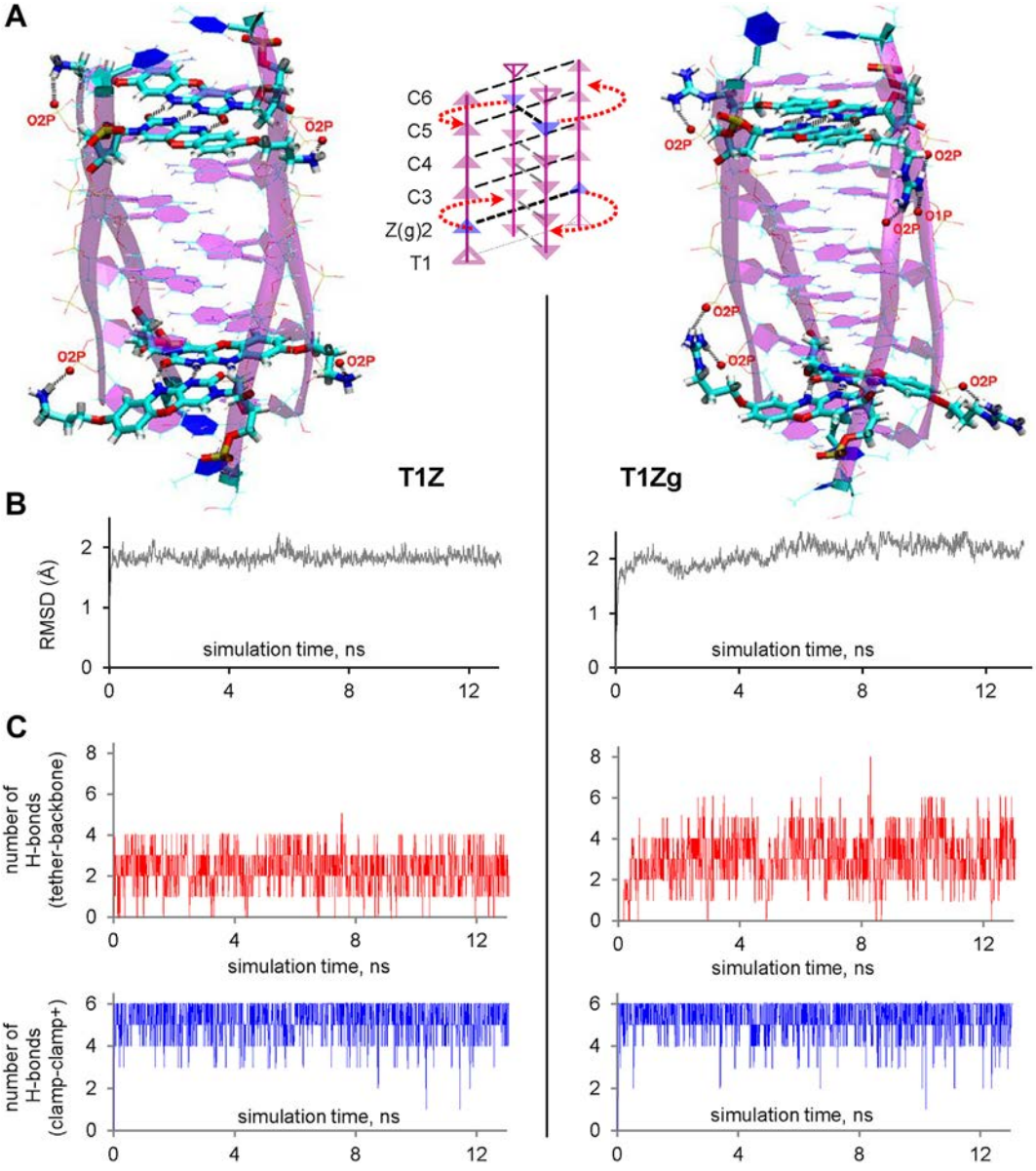

Fig. 2. i-Clamp *versus* guanidino-*i*-clamp: IM models, RMSD and H-bonding time plots (from MD simulations). A – 12-ns simulation snapshots for T1Z and T1Zg. B – RMSD time plots. C – H-bonding time plots.

obscure. This could be attributed to non-cooperative folding and/or conformational polymorphism of U1Zg.

The melting (Tm) and annealing (Ta) temperatures of all the IMs, determined from the first derivatives of the melting/annealing curves (Fig. 4C), are summarized in Table 1 and can be directly compared with the previously reported data for *i*-clamp-IMs [35]. The guanidino group did not impart profound additional stabilization. The effects of *i*-clamp and guanidino-i-clamp were very close (*e.g.*, $\Delta Tm^{T1Zg\text{-}To} = +6 \pm 2$ °C (Table 1); $\Delta Tm^{T1Z\text{-}To} = +5 \pm 2$ °C [35]). The ΔTm/Ta values coincided within the experimental error for all IMs except Uo, which may have a somewhat different folding. The 5′-terminal C → guanigino-i-clamp substitutions (T1Zg, U1Zg, M1Zg and G1Zg) were beneficial, while the 3′-terminal (M6Zg) and middle-strand (G2Zg) substitutions caused negligible and pronounced destabilization, respectively.

To clarify the basis for the effects of guanidino-*i*-clamp and analyze the pH sensitivities of the native and modified IMs in more detail, we next performed stopped flow experiments with monitoring of IM folding/unfolding by CD at 288 nm (the IM-specific CD band).

3.3. Folding/Unfolding Kinetics of i-Motifs Under Near-Physiological pH Alterations: Native Versus Clamp-Modified i-Motifs as Potential pH-Sensitive Elements for In Vivo Applications

The kinetics of IM formation have previously been studied by a number of methods, including SPR, FRET-based techniques and NMR spectroscopy [38–43] – all these methods are only applicable to relatively slow processes. Recently, stopped flow-based analyses of rapid IM folding/unfolding (typically induced by 8 → 5/5 → 8 pH jumps) have been reported [44,45]. In these studies, the pH conditions were selected to ensure complete (pseudo-irreversible) formation/disruption of the structures, which simplifies the interpretation of the kinetic curves and apparent rate constants. In the first CDSF (stopped-flow with monitoring by CD) experiments [44], the addition of highly concentrated buffers, *i.e.*, drastic changes in the solution ionic strength, was used for pH-jump implementation.

We did not aim to perform an in-depth investigation or quantitative characterization of the IM kinetics in this study. Instead, we

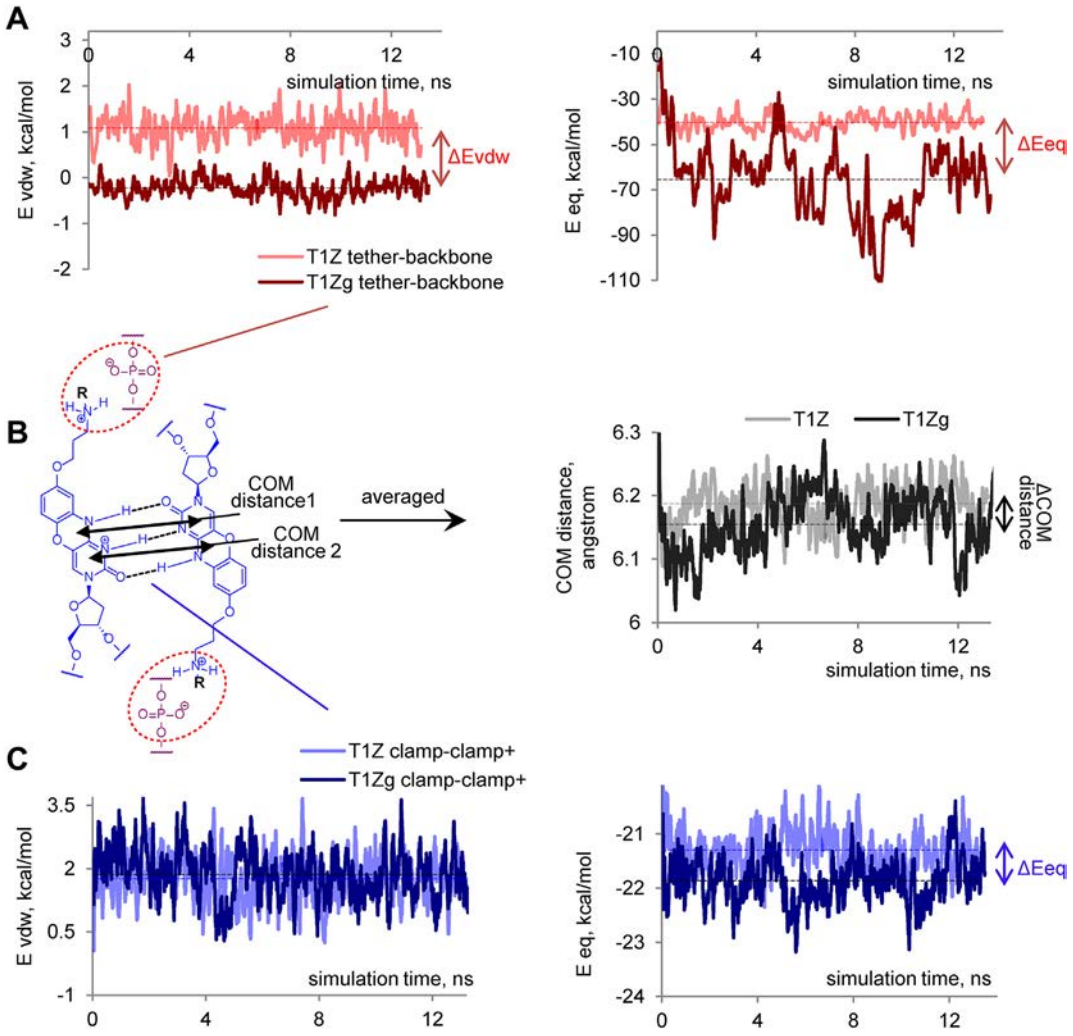

Fig. 3. i-Clamp *versus* guanidino-*i*-clamp: COM distance and energy time plots (from MD simulations). A – Electrostatic and van der Waals energy plots for tether-backbone interactions. B – Distances between phenoxazine residue COMs (centers of mass) in clamp–clamp$^+$ pairs. C – Electrostatic and van der Waals energy plots for clamp–clamp$^+$ pairs. The energy and COM distance plots were smoothed using the moving average method (span = 5).

posed the principal question of whether IM rearrangements are slow or rapid after biologically relevant moderate pH changes. We used pseudo-physiological conditions (relatively high salt concentrations) for genomic (Go) and model (Mo) IMs and their derivatives. Importantly, we designed CDSF experiments to avoid drastic changes in solution ionic strength because such changes, *per se* are known to affect IMs [5]. Four series of CDSF experiments were performed: 6.8 → 5.7 and 5.2 → 7.5 pH-jumps for To, Uo and their derivatives; 8.0 → 6.0 and 6.7 → 7.9 pH-jumps for Mo, Go and their derivatives. The pH ranges (narrowed down compared with a typical pH jump) were selected based on the previously determined transition points (pHi) of the unmodified ODNs: pHi = 7.3 ± 0.1 for Mo according to [35] or 7.1 for Mo and G0 according to [32] (slightly different buffers were used in the cited works), pHi(To) = 5.8 ± 0.1 and pHi(Uo) = 6.0 ± 0.1 [35].

The resulting kinetic curves and final-point CD spectra are shown in Fig. 5. The post-CDSF spectra of To, Uo and their derivatives at pH 5.7 (Fig. 5A) were similar in shape to those shown in Fig. 4A (pH 5.8), although the increased ionic strength in the CDSF experiments resulted in a somewhat decreased molar ellipticity of To and T1Zg near 288 nm. The post-CDSF spectra of Mo, Go and their derivatives at pH 6.0 (Fig. 5A) were rather similar to those shown Fig. 4A (pH 7.4) –IM structures (folded at least partially) were present in all cases. The post-CDSF spectra at pH 7.5 (Uo, To and their derivatives) and 7.9 (Mo, Go and their derivatives) with the CD maxima shifted to 275 nm (Fig. 5B) indicated unfolded (or mostly unfolded) ODNs.

The 6.8 → 5.7 kinetic curves obtained for To and T1Z (Fig. 5A) could not be thoroughly analyzed due to the poor signal-to-noise ratio, even though we increased the initial (pre-dilution) concentrations of these ODNs to 70 μM, which corresponds to a final ODN concentration of 15 μM after 1:4 mixing with the buffer (for other ODNs, the final concentration was 3 μM). The rest of the kinetic curves could be well fitted to single exponentials (a reduced chi squared ≈1 in all cases).

Previous studies of IM kinetics (reported for the C20T mutant of the NHEIII c-MYC promoter fragment) revealed two-step folding: rapid formation of the intermediate and its subsequent slow rearrangement [45]. For our inter- and intramolecular IMs, no clear signs of intermediates were observed. We do not exclude multi-step processes. However, even if intermediates exist, there appears to be a key limiting step that accounts for the major CD changes. The apparent rate constants determined by single-exponential fitting of the kinetic curves from Fig. 5 are given in Table 2.

As evident from the curves shown in Fig. 5 and the data presented in Table 2, the 6.8 → 5.7/8.0 → 6.0 transition kinetics were similar for native and modified IMs. The processes were fast (tau½ < 100 msec).

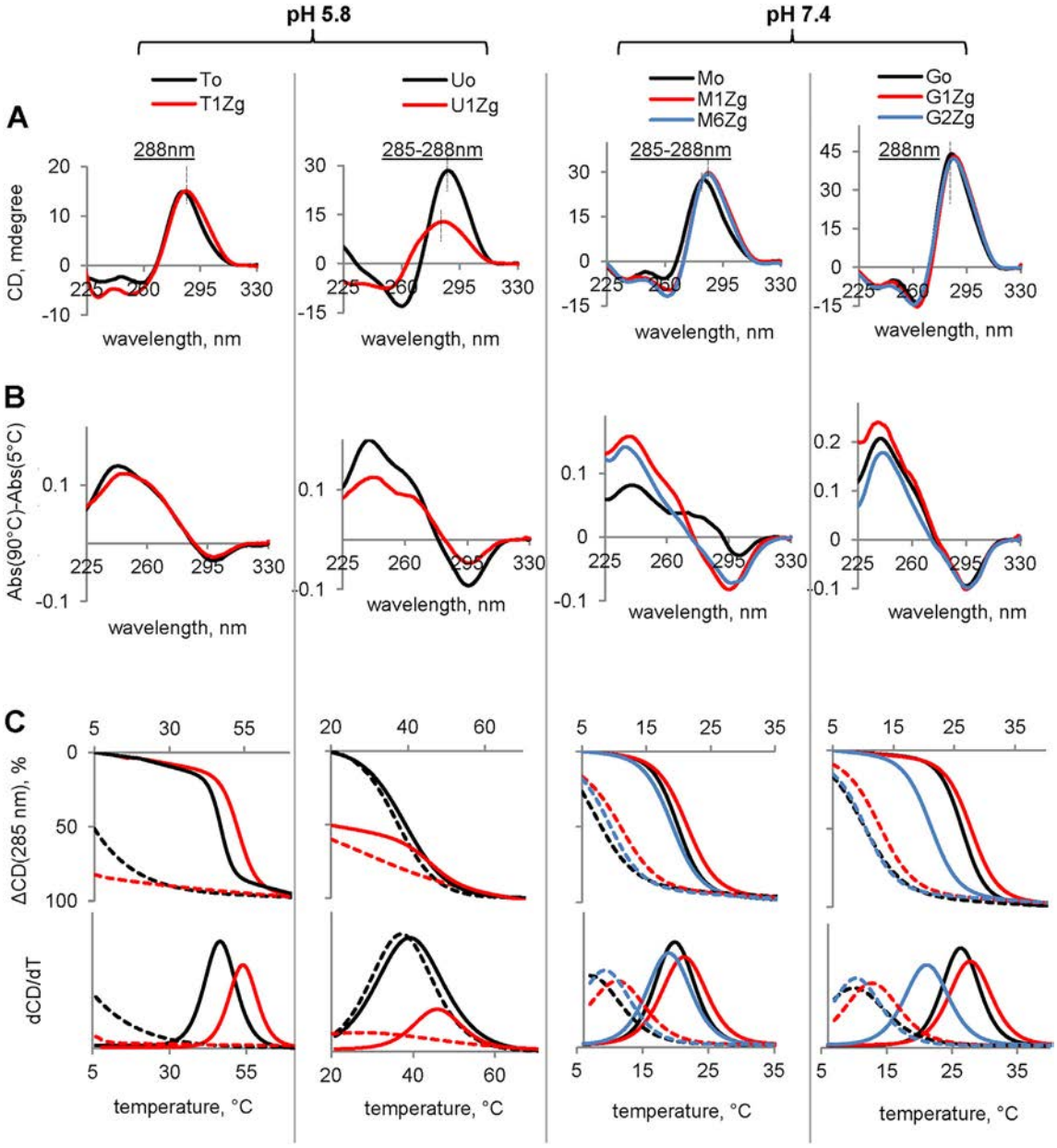

Fig. 4. IMs with guanidino-*i*-clamp insertions *versus* native IMs: characterization by optical methods. A – CD spectra at 5 °C, B – TDS, C – melting curves (solid lines), annealing curves (dashed lines) and their first derivatives. Conditions: 10 mM sodium phosphate (pH 7.4) and 100 mM NaCl (for Go, Mo and their analogues) or 10 mM sodium phosphate, pH 5.8 (for To, Uo and their analogues). ON concentrations: 10 μM (To and T1Zg) or 5 μM (the rest).

M1/M6Zg and G1/G2Zg had somewhat reduced 8.0 → 6.0 response rate constants compared with Go and Mo, respectively. We cannot postulate irreversible IM formation at the final pH, so those response rates should probably be interpreted as observed rather than actual folding rates: $K_{obs} = k_{folding}{}^{*}[ODN]^{n-1} + k_{unfolding}$, where n is the number of strands in IM. Thus, the decreased Kobs(8.0 → 6.0) of modified IMs may actually indicate slow unfolding. For the 5.2 → 7.5/6.7 → 7.9 pH jumps, a drastic decrease in the response rates was observed for all 5′-modified IMs. Interestingly, the effects of 3′-terminal (M6Zg) and middle-strand (G2Zg) modifications were much less pronounced. Again, the response rates should probably be interpreted as observed rather than actual unfolding rates because we cannot postulate total irreversible disruption of the IMs at a near-physiological pH.

Comparison of the Kobs values for the pH jumps 6.8 → 5.7/8.0 → 6.0 (folding is the dominating process, and the impact of guanidino-*i*-clamp varies from moderate to negligible) and 5.2 → 7.5/6.7 → 7.9 (unfolding is the dominating process, and the impact of 5′-terminal guanidino-*i*-clamp is profound) led us to draw the following conclusions:

- 5′-terminal modifications seem to dramatically decrease the IM unfolding rate, while other modifications cause moderate rate decreases;
- The unfolding-impeding effects may be partially (5′-modication) or totally/almost totally (3′-modification) compensated by moderate folding-impeding effects;
- In the case of middle-strand modifications, the folding slowdown seems to dominate over the unfolding slowdown.

Importantly, these kinetic data were consistent with the thermodynamic data, which indicated IM stabilization by the 5′-guanidino-*i*-clamp, a minor effect of the 3′- guanidino-*i*-clamp and destabilization by the middle-strand clamp (Table 1). The effects of

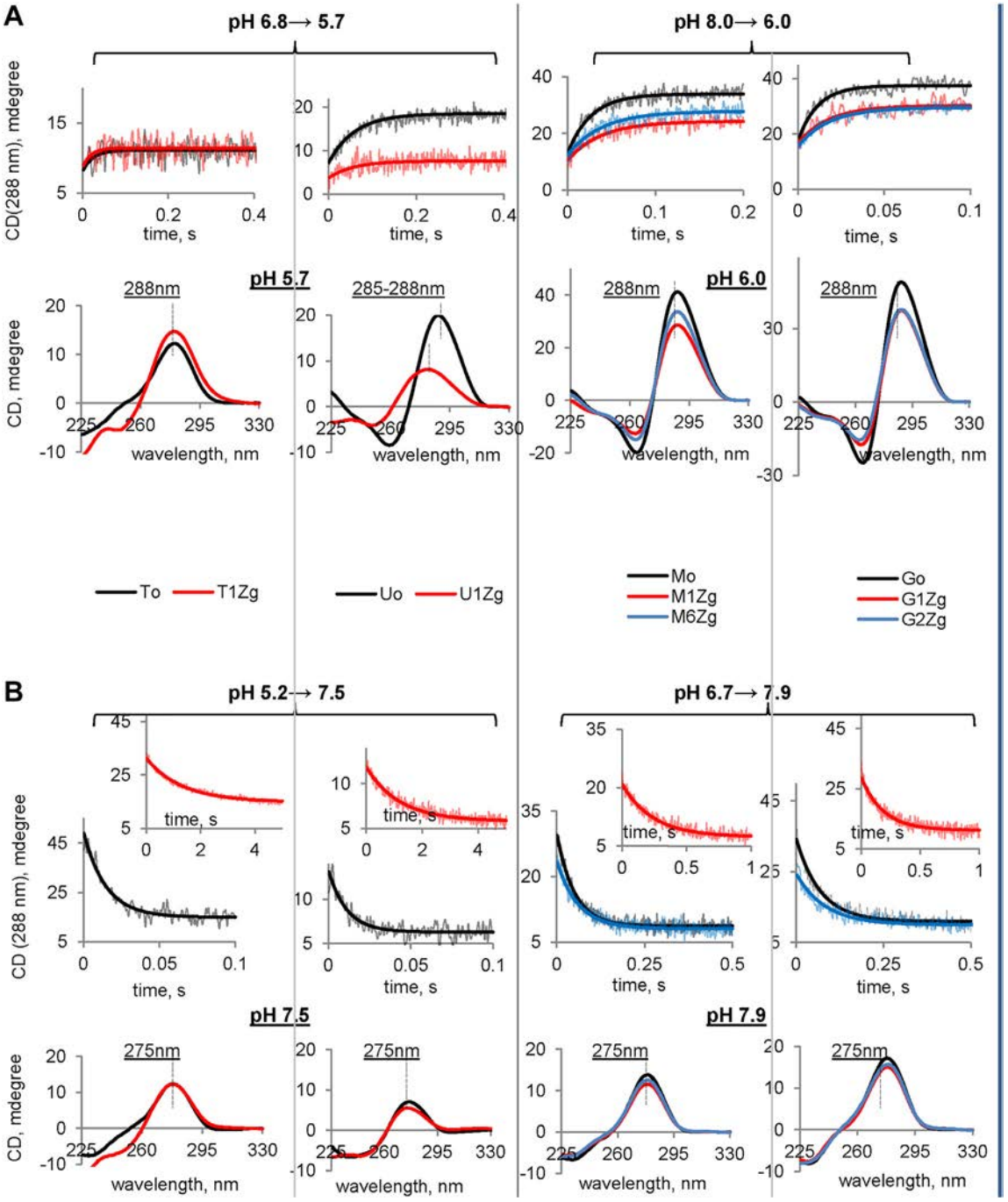

Fig. 5. IMs with guanidino-*i*-clamp insertions *versus* native IMs: CDSF results and final-point CD spectra. A – Kinetic curves obtained upon folding-facilitating pH jumps 6.8 → 5.7 (Uo, U1Zg, To and T1Zg) and 8.0 → 6.0 (Go, G1Zg, G2Zg, Mo, M1Zg and M6Zg) and the respective final-point CD spectra (conditions: 74 mM sodium phosphate, pH 5.7/6.0; 90 mM NaCl for Go, Mo and their derivatives; ODN concentrations: 15 μM for To and T1Zg; 3 μM for the rest). C – Kinetic curves obtained upon unfolding-facilitating pH jumps 5.2 → 7.5 (Uo, U1Zg, To and T1Zg) and 6.7 → 7.9 (Go, G1Zg, G2Zg, Mo, M1Zg and M6Zg) and the respective final-point CD spectra (conditions: 74 mM sodium phosphate, pH 7.5/7.9; 90 mM NaCl for Go, Mo and their derivatives; ODN concentrations: 15 μM for To and T1Zg; 3 μM for the rest). Temperature: 25 °C. A and B have joint legends.

the 5′-modification are double-sided (positive effects on stability and negative effect on kinetics). Based on the molecular modeling data, one can assume that the drastic unfolding slowdown observed for 5′-guanidino-i-clamp-IMs is due to the additional bonding between the clamp tether and the neighboring strand backbone.

With respect to potential applications of the modified IMs as core elements of pH sensors, the slowed-down kinetics are an obvious disadvantage for monitoring rapid processes, such as pH changes in neurons. However, modified IMs are still applicable for the detection of rather slow changes, such as tumor acidification or pH changes upon endosome maturation. For unmodified IMs, we demonstrated rapid responses to moderate pH changes. Rapid folding and unfolding of genomic and model (Go and Mo) IMs at a near-physiological pH and ionic strength were observed for the first time and might have physiological values. These results shed light on the possible rearrangements of IM-prone DNA fragments *in vivo* and should be helpful for the future design of genomic IM-based pH probes.

4. Conclusions

We described a new IM modification, guanidino-*i*-clamp, and have shown that it enhances IM stability upon incorporation at the 5′

Table 2
Observed constant rated obtained from monoexponential fitting of the IM kinetic curves.

ODN	K obs, s^{-1}	
	pH 6.8 → 5.7	pH 5.2 → 7.5
To	N/A[a]	68 ± 2
T1Zg	N/A	0.76 ± 0.02
Uo	17 ± 2	90 ± 5
U1Zg	17 ± 3	0.85 ± 0.03
	pH 8.0 → 6.0	pH 6.7 → 7.9
Mo	38 ± 1	20.1 ± 0.5
M1Zg	26 ± 1	4.6 ± 0.1
M6Zg	26 ± 1	12.7 ± 0.5
Go	88 ± 4	14.5 ± 0.4
G1Zg	55 ± 4	5.4 ± 0.2
G2Zg	55 ± 4	12.1 ± 0.6

[a] N/A – the kinetic curve could not be analyzed properly (low signal to noise ratio).

terminus of ODNs. Molecular modeling data suggest that guanidino-*i*-clamp is superior to the previously reported *i*-clamp (at least in terms of the tetramolecular structure with clamp–clamp$^+$ pairs) due to enhanced tether-backbone interactions, which facilitate clamp/clamp$^+$ juxtaposition and pairing. However, the difference between the stabilizing effects of *i*-clamp and guanidino-*i*-clamp on IMs is minor *in vitro*. Based on a kinetics analysis, we attribute the stabilizing effects of the 5′-terminal guanidino-*i*-clamp modifications to the decrease of the IM unfolding rate. This observation has important implications for the design of IM-based pH sensors. Modified IMs seem to be preferable only if the sensor response rate can be sacrificed for temperature tolerance. Interestingly, the apparent folding and unfolding rates of model and genomic IMs under pseudo-physiological conditions and near-physiological pH changes were moderate and high in modified and native IMs, respectively. This is the first demonstration of rapid responses of genomic IMs to pH stimuli, which supports the concept of genomic IMs being regulatory elements and encourages the future design of rapid-response pH probes based on genomic structures.

Acknowledgements

This work was supported by RFBR and Moscow city Government (grant 19-34-70004 to AMV – kinetics and molecular modeling) and Russian Science Foundation (grant 18-74-00051 to AVA – synthesis and thermal stability analysis).

Appendix A. Supplementary data

Supplementary data to this article can be found online at https://doi.org/10.1016/j.csbj.2019.04.006.

References

[1] Gehring K, Leroy JL, Gueron M. A tetrameric DNA-structure with protonated cytosine. Cytosine base-pairs. Nature 1993;363:561–5.
[2] Zeraati M, Langley DB, Schofield P, Moye AL, Rouet R, Hughes WE, et al. I-motif DNA structures are formed in the nuclei of human cells. Nat Chem 2018;10:631–7.
[3] Dzatko S, Krafcikova M, Hansel-Hertsch R, Fessl T, Fiala R, Loja T, et al. Evaluation of the stability of DNA i-motifs in the nuclei of living mammalian cells. Angew Chem Int Ed 2018;57:2165–9.
[4] Abou Assi H, Garavis M, Gonzalez C, Damha MJ. I-motif DNA: structural features and significance to cell biology. Nucleic Acids Res 2018;46:8038–56.
[5] Benabou S, Avino A, Eritja R, Gonzalez C, Gargallo R. Fundamental aspects of the nucleic acid i-motif structures. RSC Adv 2014;4:26956–80.
[6] Day HA, Pavlou P, Waller ZAE. I-motif DNA: structure, stability and targeting with ligands. Bioorg Med Chem 2014;22:4407–18.
[7] Yang B, Rodgers MT. Base-pairing energies of proton-bound heterodimers of cytosine and modified cytosines: implications for the stability of DNA i-motif conformations. J Am Chem Soc 2014;136:282–90.
[8] Fleming AM, Ding Y, Rogers RA, Zhu J, Zhu J, Burton AD, et al. 4n-1 is a "sweet spot" in DNA i-motif folding of 2'-deoxycytidine homopolymers. J Am Chem Soc 2017;139:4682–9.
[9] Protopopova AD, Tsvetkov VB, Varizhuk AM, Barinov NA, Podgorsky VV, Klinov DV, et al. The structural diversity of C-rich DNA aggregates: unusual self-assembly of beetle-like nanostructures. Phys Chem Chem Phys 2018;20:3543–53.
[10] Malliavin TE, Gau J, Snoussi K, Leroy JL. Stability of the I-motif structure is related to the interactions between phosphodiester backbones. Biophys J 2003;84:3838–47.
[11] Fujii T, Sugimoto N. Loop nucleotides impact the stability of intrastrand i-motif structures at neutral pH. Phys Chem Chem Phys 2015;17:16719–22.
[12] Rajendran A, Nakano S, Sugimoto N. Molecular crowding of the cosolutes induces an intramolecular i-motif structure of triplet repeat DNA oligomers at neutral pH. Chem Commun 2010;46:1299–301.
[13] Sun D, Hurley LH. The importance of negative Superhelicity in inducing the formation of G-quadruplex and i-motif structures in the c-Myc promoter: implications for drug targeting and control of gene expression. J Med Chem 2009;52:2863–74.
[14] Yatsunyk LA, Mendoza O, Mergny JL. "Nano-oddities": unusual nucleic acid assemblies for DNA-based nanostructures and Nanodevices. Acc Chem Res 2014;47:1836–44.
[15] Alba JJ, Sadurni A, Gargallo R. Nucleic acid i-motif structures in analytical chemistry. Crit Rev Anal Chem 2016;46:443–54.
[16] Dembska A. The analytical and biomedical potential of cytosine-rich oligonucleotides: a review. Anal Chim Acta 2016;930:1–12.
[17] Dembska A, Bielecka P, Juskowiak B. pH-sensing fluorescence oligonucleotide probes based on an i-motif scaffold: a review. Anal Methods 2017;9:6092–106.
[18] Mergny JL, Sen D. DNA quadruple helices in nanotechnology. Chem Rev Article ASAP 2019. https://doi.org/10.1021/acs.chemrev.8b00629.
[19] Heinen L, Walther A. Temporal control of i-motif switch lifetimes for autonomous operation of transient DNA nanostructures. Chem Sci 2017;8:4100–7.
[20] Wang J, Fang RC, Hou J, Zhang HC, Tian Y, Wang HT, et al. Oscillatory reaction induced periodic C-quadruplex DNA gating of artificial ion channels. ACS Nano 2017;11:3022–9.
[21] Liao WC, Lilienthal S, Kahn JS, Riutin M, Sohn YS, Nechushtai R, et al. pH- and ligand-induced release of loads from DNA-acrylamide hydrogel microcapsules. Chem Sci 2017;8:3362–73.
[22] Shi LL, Peng P, Du Y, Li T. Programmable i-motif DNA folding topology for a pH-switched reversible molecular sensing device. Nucleic Acids Res 2017;45:4306–14.
[23] Zhu JH, Kim Y, Lin HX, Wang SZ, Mirkin CA. pH-responsive nanoparticle superlattices with tunable DNA bonds. J Am Chem Soc 2018;140:5061–4.
[24] Modi S, Swetha MG, Goswami D, Gupta GD, Mayor S, Krishnan Y. A DNA nanomachine that maps spatial and temporal pH changes inside living cells. Nat Nanotechnol 2009;4:325–30.
[25] Surana S, Bhat JM, Koushika SP, Krishnan Y. An autonomous DNA nanomachine maps spatiotemporal pH changes in a multicellular living organism. Nat Commun 2011;2:340. https://doi.org/10.1038/ncomms1340.
[26] Modi S, Nizak C, Surana S, Halder S, Krishnan Y. Two DNA nanomachines map pH changes along intersecting endocytic pathways inside the same cell. Nat Nanotechnol 2013;8:459–67.
[27] Ma WJ, Yan LA, He XX, Qing TP, Lei YL, Qiao ZZ, et al. Hairpin-contained i-motif based fluorescent ratiometric probe for high-resolution and sensitive response of small pH variations. Anal Chem 2018;90:1889–96.
[28] Chen C, Song GT, Ren JS, Qu XG. A simple and sensitive colorimetric pH meter based on DNA conformational switch and gold nanoparticle aggregation. Chem Commun 2008:6149–51.
[29] Wang CX, Du Y, Wu Q, Xuan SG, Zhou JJ, Song JB, et al. Stimuli-responsive plasmonic core-satellite assemblies: i-motif DNA linker enabled intracellular pH sensing. Chem Commun 2013;49:5739–41.
[30] Cao Y, Qian RC, Li DW, Long YT. Raman/fluorescence dual-sensing and imaging of intracellular pH distribution. Chem Commun 2015;51:17584–7.
[31] Dembska A, Kierzek E, Juskowiak B. Studying the influence of stem composition in pH-sensitive molecular beacons onto their sensing properties. Anal Chim Acta 2017;990:157–67.
[32] Wright EP, Huppert JL, Waller ZAE. Identification of multiple genomic DNA sequences which form i-motif structures at neutral pH. Nucleic Acids Res 2017;45:2951–9.
[33] Kaiser CE, Van Ert NA, Agrawal P, Chawla R, Yang DZ, Hurley LH. Insight into the complexity of the i-motif and G-quadruplex DNA structures formed in the KRAS promoter and subsequent drug induced gene repression. J Am Chem Soc 2017;139:8522–36.
[34] Rogers RA, Fleming AM, Burrows CJ. Rapid screen of potential i-motif forming sequences in DNA repair gene promoters. ACS Omega 2018;3:9630–5.
[35] Tsvetkov VB, Zatsepin TS, Belyaev ES, Kostyukevich YI, Shpakovski GV, Podgorsky VV, et al. I-clamp phenoxazine for the fine tuning of DNA i-motif stability. Nucleic Acids Res 2018;46:2751–64.
[36] Wilds CJ, Maier MA, Manoharan M, Egli M. Structural basis for recognition of guanosine by a synthetic tricyclic cytosine analogue: Guanidinium G-clamp. Helv Chim Acta 2003;86:966–78.
[37] Mergny JL, Li J, Lacroix L, Amrane S, Chaires JB. Thermal difference spectra: a specific signature for nucleic acid structures. Nucleic Acids Res 2005;33:e138. https://doi.org/10.1093/nar/gni134.
[38] Mergny JL. Fluorescence energy transfer as a probe for tetraplex formation: the i-motif. Biochemistry 1999;38:1573–81.
[39] Phan AT, Mergny JL. Human telomeric DNA: G-quadruplex, i-motif and Watson-crick double helix. Nucleic Acids Res 2002;30:4618–25.
[40] Canalia M, Leroy JL. Structure, internal motions and association-dissociation kinetics of the i-motif dimer of d(5mCCTCACTCC). Nucleic Acids Res 2005;33:5471–81.

[41] Zhao Y, Zeng ZX, Kan ZY, Hao YH, Tan Z. The folding and unfolding kinetics of the i-motif structure formed by the C-rich strand of human telomere DNA. Chembiochem 2005;6:1957–60.
[42] Leroy JL. The formation pathway of i-motif tetramers. Nucleic Acids Res 2009;37:4127–34.
[43] Lieblein AL, Buck J, Schlepckow K, Furtig B, Schwalbe H. Time-resolved NMR spectroscopic studies of DNA i-motif folding reveal kinetic partitioning. Angew Chem Int Ed 2012;51:250–3.
[44] Chen C, Li M, Xing YZ, Li YM, Joedecke CC, Jin J, et al. Study of pH-induced folding and unfolding kinetics of the DNA i-motif by stopped-flow circular dichroism. Langmuir 2012;28:17743–8.
[45] Reilly SM, Lyons DF, Wingate SE, Wright RT, Correia JJ, Jameson DM, et al. Folding and hydrodynamics of a DNA i-motif from the c-MYC promoter determined by fluorescent cytidine analogs. Biophys J 2014;107:1703–11.